ACS NANO
Cite This: ACS Nano 2019, 13, 3796–3805
www.acsnano.org

ARTICLE

Crab-on-a-Tree: All Biorenewable, Optical and Radio Frequency Transparent Barrier Nanocoating for Food Packaging

Taehyung Kim,[†,⊥] Thang Hong Tran,[‡,§,⊥] Sung Yeon Hwang,[‡,§] Jeyoung Park,[‡,§] Dongyeop X. Oh,[*,‡,§] and Byeong-Su Kim[*,∥]

[†]Department of Energy Engineering, Ulsan National Institute of Science and Technology (UNIST), 50 UNIST-gil, Ulsan 44919, Republic of Korea

[‡]Research Center for Bio-Based Chemistry, Korea Research Institute of Chemical Technology (KRICT), Ulsan 44429, Republic of Korea

[§]Advanced Materials and Chemical Engineering, University of Science and Technology (UST), Daejeon 34113, Republic of Korea

[∥]Department of Chemistry, Yonsei University, Seoul 03722, Republic of Korea

Supporting Information

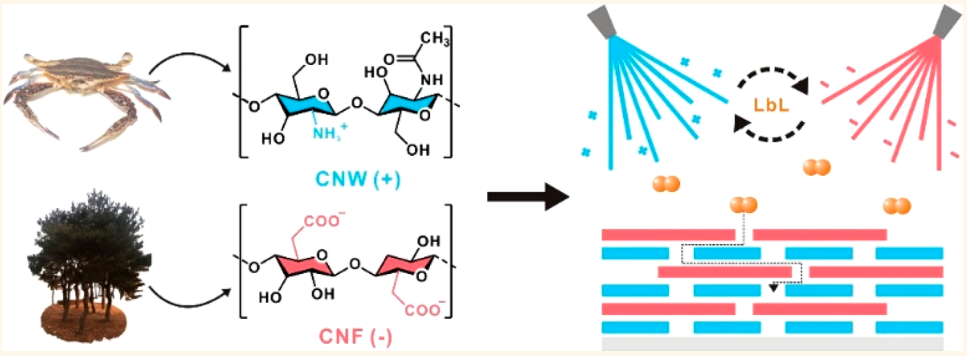

ABSTRACT: **Plastic packaging effectively protects foods from mechanical, microbial, and chemical damage, but oxygen can still permeate these plastics, degrading foods. Improving the gas barrier usually requires metallic or halogenated polymeric coatings; however, both cause environmental concerns and metallic coatings block visible light and electromagnetic signals. This paper reports a design of a highly flexible, visible light and radio frequency transparent coating on commercial poly(ethylene terephthalate) (PET) film. Nanoscale blending was achieved between negatively charged cellulose nanofibers and positively charged chitin nanowhiskers by employing spray-assisted layer-by-layer assembly. Synergetic interplay between these highly crystalline nanomaterials results in a flexible film with superior barrier characteristics. The oxygen transmission rate was below 0.5 mL m^{-2} day^{-1}. Moreover, this coating maintains its performance even when exposed to common hazards such as bending stress and hydration. The coating also notably reduces the haziness of PET with a negligible loss of transparency and provides effective inhibition of antibacterial growth. This "crab-on-a-tree" nanocoating holds high potential for biorenewable and optical and radio frequency transparent packaging applications.**

KEYWORDS: *food packaging, high-performance coating, nanomaterial, biomass, layer-by-layer assembly*

Food packaging is used to protect foods from chemical, biological, and mechanical damage. Plastics are ideal packaging materials, as their viscoelasticity protects the product against tolerable mechanical shocks, and they are generally resistant to microorganisms and chemical damage. Poly(ethylene terephthalate) (PET) and polyethylene (PE) are commonly used owing to their low cost and good moldability. However, these plastics are mostly permeable to oxygen and thus fail to prevent quality losses by oxidation. To improve the gas barrier properties, coatings consisting of either metals, metal oxides, and chlorinated polymers such as poly(vinylidene chloride) (PVDc) have been applied to the plastic films. Nevertheless, their constituents often give rise to environmental and health concerns.[1] Moreover, coatings comprising

Received: November 7, 2018
Accepted: March 11, 2019
Published: March 11, 2019

DOI: 10.1021/acsnano.8b08522
ACS Nano 2019, 13, 3796–3805

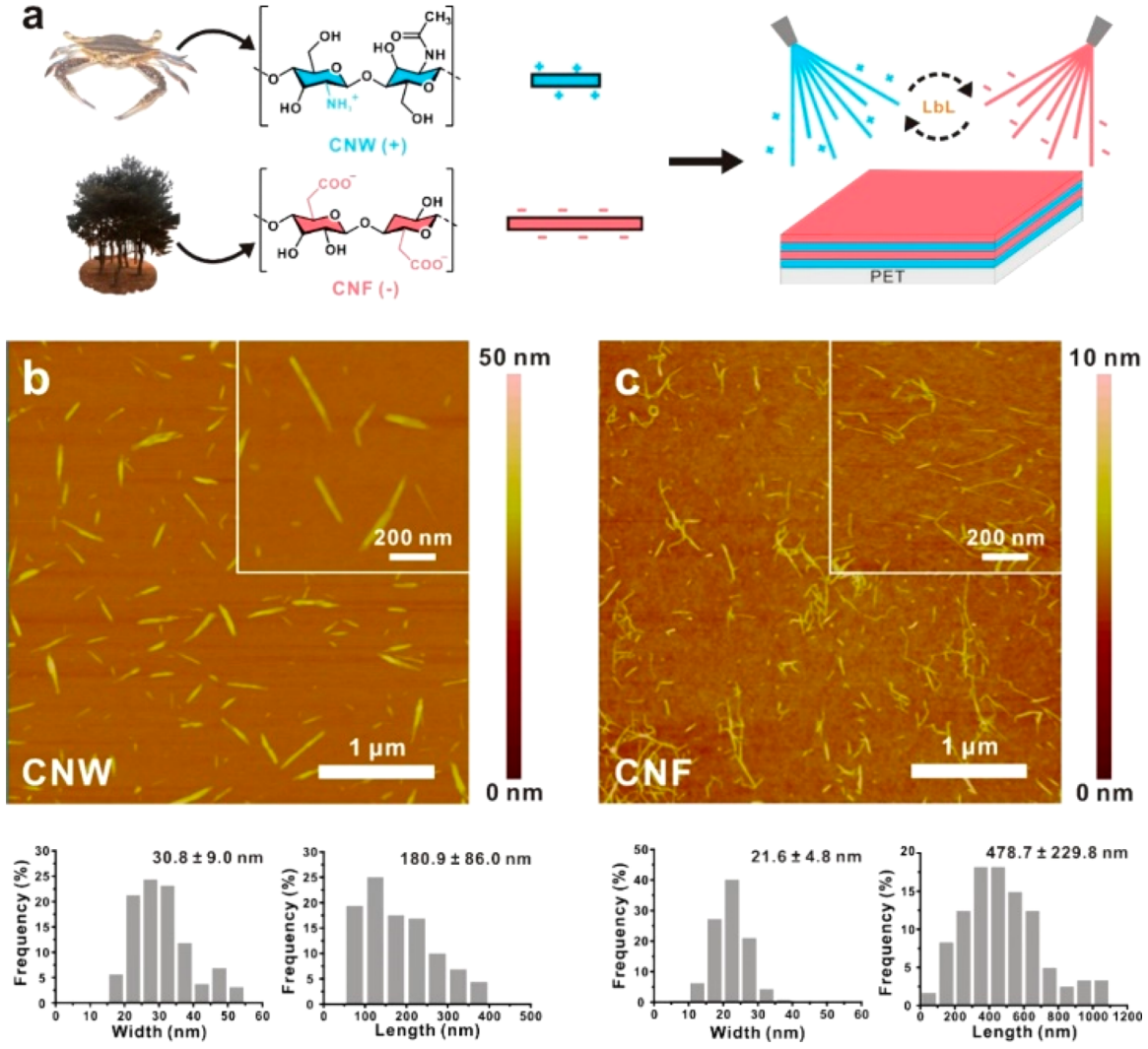

Figure 1. (a) Schematic representation of crab-on-a-tree nanocoating: Spray LbL-assembled gas barrier film on PET. Representative AFM images with the corresponding size distribution of (b) CNW and (c) CNF.

metals and metal oxides block the transmission of visible light and radio signals as well as causing the packaging to lose transparency, which also hinders its use as a next-generation "intelligent" packaging material, as optical and radio transparency will be required for effective tracking with quick response (QR) and radio frequency identification (RFID) scanners, as well as communication with smart appliances such as refrigerators that track their inventory. Thus, it is necessary to find next-generation barrier materials that are renewable, biofriendly, easily processable, and transparent to visible light and radio frequencies.[2]

Cellulose and chitin are the two most naturally abundant biopolymers. This abundance is accompanied by advantages such as renewability, biodegradability, and a high degree of crystallinity. Despite these attractive properties, they have not found widespread use owing to difficulties in solubilization and processing arising from strong interchain hydrogen bonding and van der Waals interactions. Various mechanical and chemical approaches have been followed in an attempt to address these challenges.[3−6] Interestingly, these modifications succeeded in retaining the crystallinity of the materials such that an oxygen barrier with the necessary properties was obtained. Generally, cellulose nanofibers (CNFs) prepared with both chemical (*e.g.*, 2,2,6,6-tetramethylpiperidinyloxy (TEMPO)-based oxidation) and mechanical treatments are known to achieve a higher oxygen barrier property than those prepared by only mechanical treatment.[7−9] Chemically modified CNFs have a higher degree of fibrilization and homogeneity than pristine CNFs. In this regard, chemically modified CNF forms a more dense and uniform coating. As a notable example, Isogai and co-workers reported the application of chemically modified CNFs as an effective oxygen barrier.[10] In another noteworthy effort, Meredith and co-workers chemically modified a chitin analogue to obtain a transparent, flexible material with low gas permeability.[11]

Layer-by-layer (LbL) assembly has been widely used as a versatile method to fabricate thin films with controlled architecture and composition.[12] The LbL assembly is typically achieved by the sequential deposition of oppositely charged components by strong electrostatic interactions. Because of its simplicity and versatility, LbL assembly has rapidly emerged as a platform technique for the construction of hybrid thin-film coatings with the desired architectures to form functional thin films. In this context, Grunlan and co-workers made a significant contribution to the development of a gas barrier layer by employing the LbL approach to assemble various

DOI: 10.1021/acsnano.8b08522
ACS Nano 2019, 13, 3796−3805

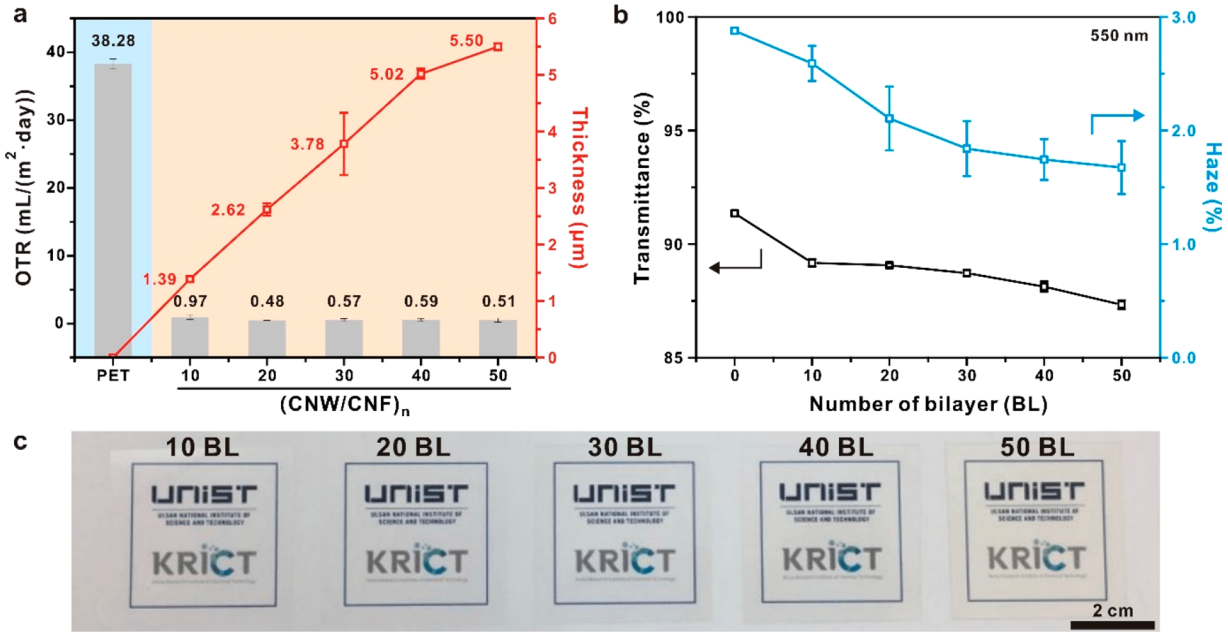

Figure 2. (a) Thickness and OTR values of PET and (CNW/CNF)$_n$ nanocoated PET with different number of bilayers. (b) Changes in transmittance and haze as a function of the number of bilayers. The values were obtained at 550 nm with 9 independent measurements. (c) Photographic images of (CNW/CNF)$_n$-coated PET films with different numbers of BLs. Background logos are used with permission from UNIST and KRICT.

nanomaterials, including graphene oxide, nanoclay, and polymer.[13−16] Despite the significant progress made thus far, there is still a need for materials that meet the highly stringent requirements of food packaging.

Herein, we report the fabrication of biomaterial-based, flexible, transparent, and gas impermeable films assembled by the spray-assisted LbL assembly of CNFs and chitin nanowhiskers (CNWs) (Figure 1a). The assembled multilayer coating significantly improved the oxygen transmission rate (OTR) compared to the individual components, suggesting synergistic interplay between the components within the multilayers. Moreover, the flexible coating displayed highly visible and radio transparency with low haziness, and even exhibited antibacterial properties. Considering the natural abundance of the raw materials, coupled with the opportunities presented by spray LbL assembly, we anticipate that this "crab-on-a-tree" coating approach will be successfully applied for transparent food packaging.

RESULTS AND DISCUSSION

Initially, CNW derived from α-chitin was prepared *via* acidic hydrolysis by using an aqueous hydrogen chloride solution, and its surface was deacetylated by an aqueous NaOH solution.[17,18] As a result of the rich amine groups along the backbone of each CNW, they possessed positive charges with a ζ-potential of +33 mV at pH 3.6 under deposition conditions. Furthermore, atomic force microscopy (AFM) indicated the average dimension of the prepared CNWs were 180.9 ± 86.0 nm in length and 30.8 ± 9.0 nm in width, respectively (Figure 1b).

In parallel, CNF was prepared using wood pulp as a cellulose source, which was oxidized in an aqueous sodium hypochlorite (NaClO) solution at pH 10 with the aid of an oxidant (see Methods for details). Oxidation minimally damages the nanofiber structure and transforms the primary hydroxyl groups on the nanofiber surface into carboxylate groups. Subsequent mechanical disintegration using a homogenizer afforded a stable CNF suspension with a ζ-potential of −47 mV at pH 7.0. The prepared CNFs were considerably longer than the CNWs, with the average length of 478.7 ± 229.8 nm, but with a similar width of 23.0 ± 4.1 nm (Figure 1c). The complementary charges of the positive CNWs and negative CNFs are expected to facilitate the formation of a multilayer thin-film coating. Moreover, the difference in their respective dimensions will aid to form tight networks in which the large CNFs provide a rigid framework, and the smaller CNWs fill local defects within the CNF meshes such as holes and voids.

The stable CNF and CNW suspensions were deposited sequentially onto commercial PET substrates (thickness of 50 μm) using a spray-assisted LbL method (Figure 1a). Gas barrier coatings were formed with multilayers of (CNW/CNF)$_n$ (where n represents the number of bilayers (BLs), typically ranging from 10 to 50 BL). Spray-assisted LbL assembly creates a relatively thicker coating compared to the more time-consuming immersion-based LbL assembly[19] and can achieve large-area coverage, which makes it one of the most relevant LbL methods for further translation into industrial applications.[20]

In a preliminary endeavor to maximize the OTR value of the coating while providing the required transparency, the spray LbL conditions were first optimized to determine the appropriate suspension concentration and substrate temperature to evaporate water droplets without leaving stains. The control sample, a bare PET substrate, had an OTR value of 31.85 ± 0.29 mL m^{-2} day^{-1}; however, this pristine OTR value increased marginally to 38.28 ± 0.74 mL m^{-2} day^{-1} after the film was subjected to the heat applied during the coating procedure. This observation can be attributed to the enhanced chain disorder of PET upon exposure to heat, as the PET segments deviate from their original, drawn-out orientation that is imposed to maximize its mechanical properties.[21] Conversely, the OTR value of LbL-coated PET films gradually

DOI: 10.1021/acsnano.8b08522
ACS Nano 2019, 13, 3796−3805

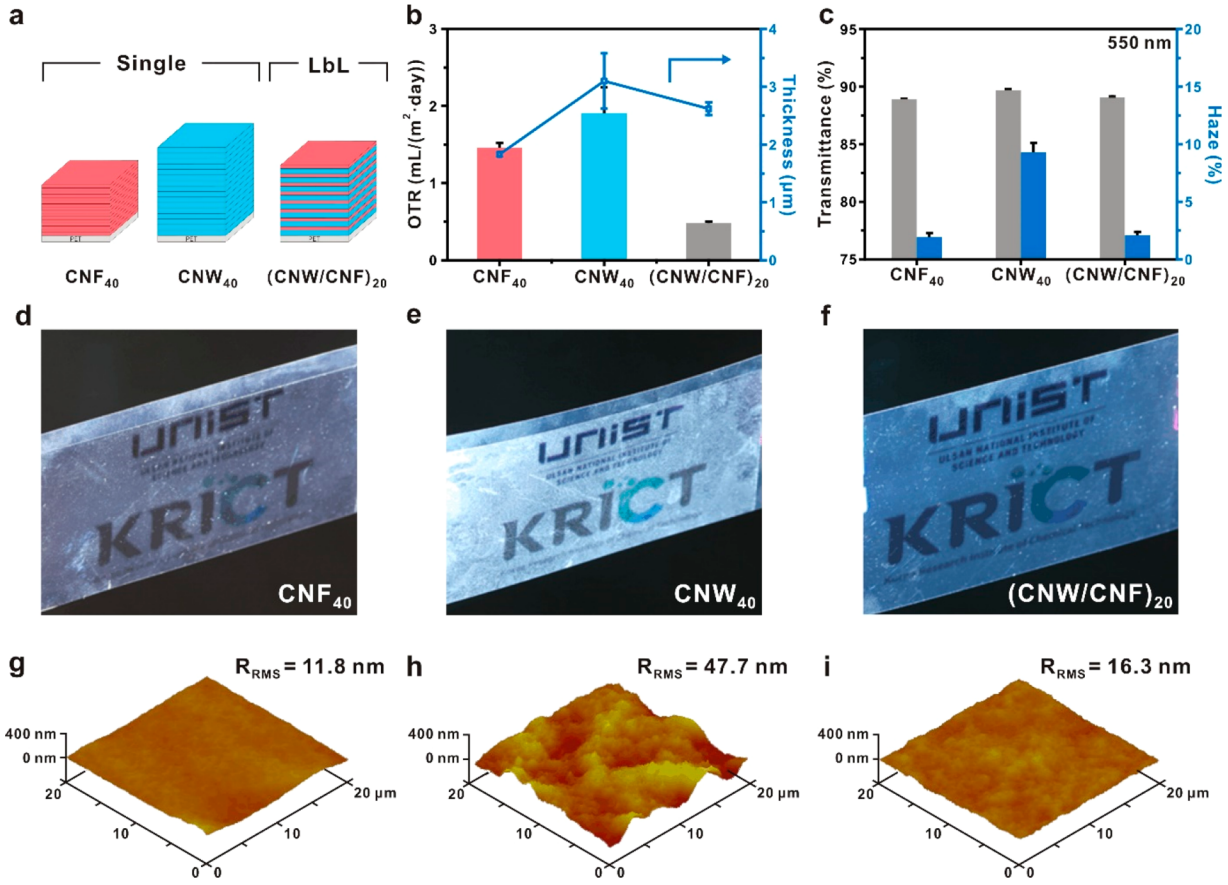

Figure 3. (a) Schematic representation of the samples prepared to elucidate the synergistic interplay of CNW and CNF at a fixed 20 BL: CNF_{40}, CNW_{40}, and $(CNW/CNF)_{20}$, (b) OTR values, and (c) light transmittance and haziness measured at 550 nm. (d–f) Rear projected holographic images on CNF_{40}, CNW_{40}, and $(CNW/CNF)_{20}$-coated PET films. (g–i) AFM image with the corresponding roughness analysis (R_{rms}) of CNF_{40}, CNW_{40}, and $(CNW/CNF)_{20}$. Background logos are used with permission from UNIST and KRICT.

decreased as the drying temperature increased (Figure S1). Apart from the enhanced chain disorder of PET, this phenomenon is due to the aggregation of sprayed CNF and CNW during water droplet evaporation. As the droplets evaporate, capillary convection resulting from the high surface tension of water pulls the nanostructures together. Whereas slow evaporation below 80 °C allows sufficient time for capillary convection to aggregate the nanostructures, fast evaporation above 80 °C does not. As a result, the drying temperature of spray-assisted LbL coating was optimized to 80 °C.

We then investigated the effect of coating thickness on OTR, transparency, and haziness (Figure 2). As expected, the thickness of a multilayer film of $(CNW/CNF)_n$ determined by a profilometer increased linearly with respect to the number of bilayers, suggesting nanoscale blending of the respective components within the multilayer. The average bilayer thickness was approximately 110 nm. Upon $(CNW/CNF)_n$ coating, the OTR value of the PET films decreased sharply to below 1.0 mL m^{-2} day^{-1} (*vs* 38.28 ± 0.74 mL m^{-2} day^{-1} for the pristine PET substrate). This enhanced oxygen barrier performance was reduced and almost saturated to 0.48 ± 0.02 mL m^{-2} day^{-1} at 20 BL. Unlike other reports, in which the OTR value decreased continuously as the film thickness increased, we speculate that this is an intrinsic limitation of fibrous CNF-based materials. Few papers have reported OTR values below 0.5, even with CNF-based films that are tens of micrometers thick (see Table S1). Despite such an intrinsic limitation, this OTR value is as high as that of a 40 nm-thick Al coating on PET,[22,23] as well as pristine polymers such as PVDc[24] and ethylene vinyl alcohol (EVOH).[25] Moreover, it complies with most food packaging requirements.[7] It is of note that considerably thicker coatings are necessary to achieve equivalent performance for PVDc (5 μm) and EVOH (5–24 μm).[24,26]

The transparency of the coated PET gradually decreased with the number of bilayers, as quantitatively expressed by the light transmittance at 550 nm (Figure 2b). Nevertheless, a high transmittance of more than 87.5% was still measured, as shown in Figure 2c. In particular, the apparent transparency reduction of the coating comprising 20 BLs is insignificant, at approximately 2% at 550 nm. Based on the Beer–Lambert law, the light transmittance of the $(CNW/CNF)_n$-coated PET film can correlate with the difference in the absorption coefficients of PET and $(CNW/CNF)_n$ and the film thickness. The reduction in transmittance is mainly due to the increase in coating thickness. However, unlike the similar values of the absorption coefficient of the $(CNW/CNF)_n$ films in the range of 220.1–244.1 cm^{-1}, the large difference in the absorption coefficients of the $(CNW/CNF)_{10}$ and PET films (223.0 *vs* 180.8 cm^{-1}) provides optical attenuation, resulting in a larger reduction in transparency. Thus, the visible light transmittance at 550 nm decreased slightly from 91% to 87% as the number of BLs increased up to a thickness of 5.5 μm (Figure S2).

DOI: 10.1021/acsnano.8b08522
ACS Nano 2019, 13, 3796–3805

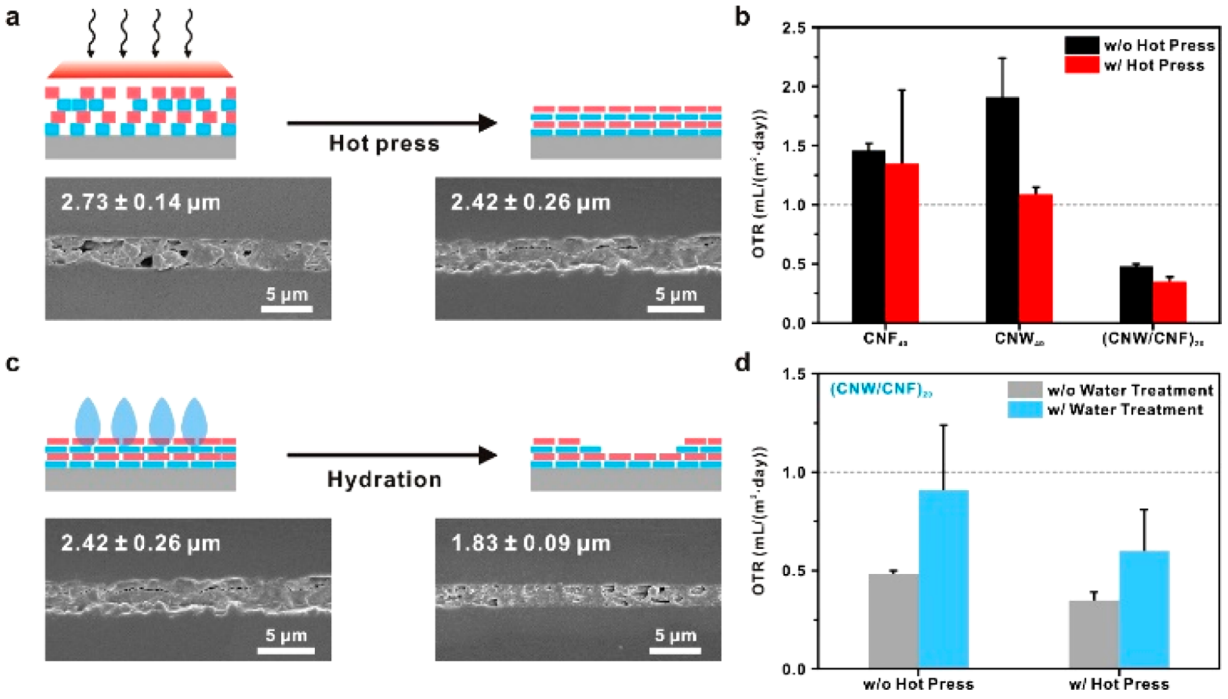

Figure 4. (a) Schematic representation of hot-pressing process of $(CNW/CNF)_{20}$ with corresponding cross-sectional SEM images. (b) Changes in OTR values of CNF_{40}, CNW_{40}, and $(CNW/CNF)_{20}$ nanocoating before and after hot-pressing. (c) Schematic representation of hot-pressed $(CNW/CNF)_{20}$ before and after hydration with corresponding cross-sectional SEM images. (d) Changes in OTR values of $(CNW/CNF)_{20}$-coated PET films after water submersion. The thickness of the nanocoating was determined at 20 different points on the samples.

Moreover, it is worth noting that the transparency reduction by crab-on-a-tree nanocoating is significantly low compared to the inorganic gas barrier coating of graphene derivatives[27] and aluminum,[28] both of which have an absorption coefficient larger than 10^5.

In food packaging applications, haziness often distorts a consumer's perception of quality.[29] Thus, the effects of nanocoating on the haziness of PET were evaluated. Interestingly, in contrast to the general trend, the haziness decreased linearly with the number of BLs, as quantitatively measured at 550 nm (Figure 2b). The reduced light scattering of the coated PET compared to the bare PET can be attributed to the reduction in surface roughness as determined by AFM (Figure S3).

The synergistic effects of CNW and CNF on the performance of the gas barrier and optical properties of the $(CNW/CNF)_n$ coating were further evaluated in comparison with the respective individual components (Figure 3a). For example, $(CNW/CNF)_{20}$ was compared with single component coatings CNW_{40} and CNF_{40}. The single component coatings were prepared under identical spraying conditions to the bilayer coatings, but with only one suspension. Interestingly, both the CNW_{40} and CNF_{40}-coated PET films presented much higher OTR values of 1.91 ± 0.33 mL m^{-2} day^{-1} (**$p < 0.01$) and 1.46 ± 0.06 mL m^{-2} day^{-1} (***$p < 0.005$), respectively, than that of $(CNW/CNF)_{20}$-coated PET (0.48 ± 0.02 mL m^{-2} day^{-1}) (Figure 3a). The synergistic combination of CNW and CNF improves the oxygen barrier performance owing to ionic cross-linking between the respective amine and carboxylate groups, which reduces the free volume in the film. This is also reflected in the considerable thickness reduction of the $(CNW/CNF)_{20}$ nanocoating. Moreover, the dimensional difference between the CNWs and CNFs produces a tight packing in which local defects in the larger CNF-based fibrous system are filled with the smaller CNW particles.

The optical properties of CNW_{40}, CNF_{40}, and $(CNW/CNF)_{20}$-coated PET films are compared in Figure 3c–f. Although none of the coatings severely diminished the transparency of PET (all the values exceed 85% in the visible range), CNF_{40} and $(CNW/CNF)_{20}$-coated PET yielded a significantly lower haziness of 0.8%, in clear contrast to that of CNW_{40}-coated PET. The haziness was further visualized by capturing rear-projected holographic images (Figure 3d–f). The high degree of haziness of CNW_{40}-coated PET could be correlated with the high surface roughness, arising from the non-uniform coating of rigid CNW, as determined from AFM (Figure 3h).

The synergistic interplay of CNW and CNF arising from the electrostatic interactions can be further strengthened by subjecting the films to hot-pressing treatment at 80 °C at 30 MPa for 10 min. The FT-IR spectra of the $(CNW/CNF)_{20}$-coated PET revealed the formation of amide bonds between CNF and CNW, as evidenced by the increased intensity of the amide I peak at 1655 cm^{-1} with a concomitant shift of the amide II peak from 1560 to 1554 cm^{-1}. Conversely, these changes were absent in the control sets of CNW_{40} CNW_{40} and CNF_{40} (Figure S4). This observation confirms the formation of amide bonds creating ionic cross-links, and thus increased packing of CNW and CNF upon hot-pressing.[30] As a result, hot pressing further improves the gas barrier property as well as the hydration resistance necessary for food packaging. As shown in the cross-sectional SEM image of the nanocoated film in Figure 4a, hot-pressing treatment compressed the film by 11.4%, which resulted in a reduction in the size and number of pores within the nanocoating. Thus, these tighter

DOI: 10.1021/acsnano.8b08522
ACS Nano 2019, 13, 3796–3805

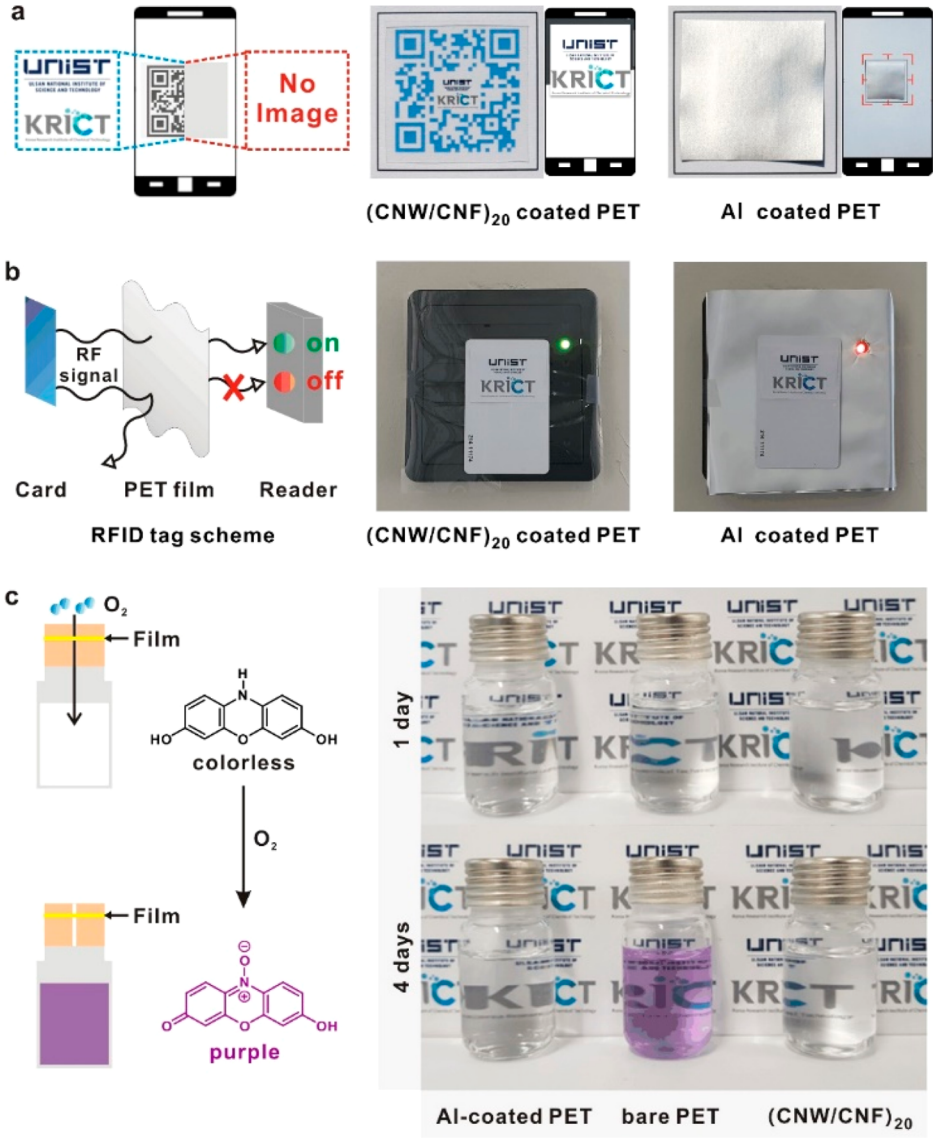

Figure 5. Optical/digital capability of crab-on-a-tree-coated PET to transmit information. (a) QR code reading underneath $(CNW/CNF)_{20}$ and Al-coated PET film, (b) RFID tag reading by a RF reader through $(CNW/CNF)_{20}$ and Al-coated PET film. (c) Color changes of resazurin solution under Al-coated PET (control), bare PET, and $(CNW/CNF)_{20}$-coated PET. Background logos are used with permission from UNIST and KRICT.

intercomponent networks formed after hot pressing more effectively blocked the oxygen pathway in the $(CNW/CNF)_{20}$ coating. This is corroborated by the improvement in OTR compared to that before the treatment (0.35 ± 0.04 mL m^{-2} day^{-1} [$^*p < 0.05$] *vs* 0.48 ± 0.02 mL m^{-2} day^{-1}). In comparison, the hot-pressing treatment also benefited the CNW_{40} coating ($^*p < 0.05$), but not as much as the CNF_{40} coating (not significant, $p > 0.05$). This could possibly be attributed to the greater thickness of the CNW coating and the higher degree of free volume within the coating.

To assess their performance in wet and humid conditions, the bare and hot-pressed $(CNW/CNF)_{20}$-coated PET films were subjected to extreme hydration conditions by submersion in water for 1 h. As shown in the cross-sectional SEM image in Figure 4c, the water treatment reduced the film thickness and gave rise to small-sized pores, probably because a portion of the nanocoating was washed away. The non-hot-pressed $(CNW/CNF)_{20}$-coated PET film exhibited an increase in the OTR to 0.91 ± 0.33 mL m^{-2} day^{-1} (Figure 4d) compared to the hot-pressed $(CNW/CNF)_{20}$-coated PET (see SEM images in Figure S5). Surprisingly, however, the hot-pressed PET sample retained its OTR of 0.60 ± 0.21 mL m^{-2} day^{-1} (not significant, $p > 0.05$) in comparison to the original OTR of 0.35 ± 0.04 mL m^{-2} day^{-1} (Figure 4d). This suggests that the weakly packed nanostructures that were washed away contributed marginally to the gas barrier property. Notably, conventional EVOH coatings display a high OTR of ~10 mL m^{-2} day^{-1} at a relative humidity of 80% atmosphere without direct contact with water due to hydration of the hydroxyl groups.[31]

Food packaging experiences external mechanical stresses during actual usage. As a model study, the hot-pressed $(CNW/CNF)_{20}$-coated PET films were repeatedly folded and unfolded 200 times using a bending tester (Figure S6). Although the OTR of both the hot-pressed and non-treated samples increased slightly to 1.02 ± 0.05 ($^{***}p < 0.005$) and 1.27 ± 0.14 mL m^{-2} day^{-1} ($^*p < 0.05$), respectively, the values still fulfill the OTR requirement (typically <1 mL m^{-2} day^{-1} for

DOI: 10.1021/acsnano.8b08522
ACS Nano 2019, 13, 3796−3805

most types of foods).[7] Moreover, the bending stress did not give rise to the formation of cracks as shown in Figure S7. Taken together, this observation demonstrates that effective ionic cross-linking within the multilayer contributes to mechanical stability of the coating. Further tests were performed for the representative $(CNW/CNF)_{20}$ films after exposure to various harsh conditions: (1) 1 year aging; (2) freezing at −20 °C; (3) exposure to ethanol; and (4) heating in a microwave oven (Figure S8). Interestingly, most of these harsh environments did not significantly degrade the integrity of our barrier film, as evidenced by the appearance and the OTR values of the films. An exception to this was the film treated in the microwave oven, which showed a slightly increased OTR value of 1.11 ± 0.07 mL m^{-2} day^{-1}. Nevertheless, it is still encouraging, considering that customers usually discard food packaging before or after microwave treatment.

Next-generation food packaging should appeal to consumers and distributors and should not only allow a clear view of the contents but also the detailed information of the contents to be obtained. Thus, securing visual validation through packaging with high transparency and low haziness enhances the shelf appeal of products. Our transparent crab-on-a-tree coating not only satisfies the aforementioned requirements, it also guarantees the use of digitally readable optical labels such as QR codes (Figure 5a). This is in clear contrast to conventional Al coatings on PET films, which prevent the passage of visible light.

Next-generation "intelligent" food packaging will be required to interact with the Internet-of-Things (IoT). The packaging will be embedded with a radio frequency (RF) tag to enable it to be tracked and monitored by an RF reader in a refrigerator or inventory.[32] However, conductive materials can generate electromagnetic RF shielding, so the performance of RF communication will be inversely proportional to the conductivity of the packaging material.[33] As a proof-of-concept, the $(CNW/CNF)_{20}$-coated PET film was placed between an RF tag and its reader (Figure 5b). As expected, the tag on the opposite side of the nonconductive crab-on-a-tree-coated PET film was readable, as indicated by the green light, whereas the tag could not be read through the conductive Al-coated PET. It should be noted that, although graphene derivatives and related two-dimensional nanomaterials are regarded as good candidates for gas barrier coatings, their performance in RF-based tracking applications would be inferior to the crab-on-a-tree coating owing to their high electromagnetic shielding performance.[33] Figure 5c presents a visualization of the oxygen barriers in bare and $(CNW/CNF)_{20}$-coated PET. The visualization test was conducted for a period of 4 days with Al-coated PET samples as the control group. After 4 days, only the bare PET sample changed to pink, whereas the Al-coated PET sample and $(CNW/CNF)_{20}$-coated PET remained colorless. This indicates that the oxygen barrier of the crab-on-a-tree coating is as effective as that of Al-coated PET under the examined conditions.

Antibacterial properties are another attractive function for food packaging applications. As chitin is well-known for its antibacterial properties,[34] we examined the antibacterial properties of the crab-on-a-tree-coated PET upon incubation with suspensions of *Escherichia coli* and *Bacillus subtilis* (Figure S9). Regrowth of the bacterial cells was evaluated by measuring the OD_{600}, which showed that the bacterial cells were effectively inhibited in the order of CNW_{40}, $(CNW/CNF)_{20}$, CNF_{40}, and bare PET. As expected, the extent to which the bacterial growth was inhibited was affected by the CNW content based on the nature of chitin. In both cases, the crab-on-a-tree coating inhibited bacterial growth, because the OD of the $(CNW/CNF)_{20}$ PET medium was 3.5-fold lower than that of the bare PET medium. Interestingly, the CNF_{40} coating also mildly inhibited bacterial growth on the surface. This finding was attributed to repulsion of cell membrane by the negative charges of CNF, thereby hindering the settlement of bacterial cells on the substrate.[35,36] In addition, *in vitro* cytotoxicity of the crab-on-a-tree coating to a mammalian cell line (MC3T3-E1) was examined *via* colorimetric assay with an empty well (no film), bare PET, and the $(CNW/CNF)_{20}$-coated PET (Figure S10). No significant difference was indicated in the number of viable cells among them ($p > 0.05$), implying that the crab-on-a-tree coating exhibited no cytotoxicity toward the MC3T3-E1 cells.

CONCLUSION

In conclusion, we developed a biomaterial-based, transparent, and flexible gas barrier coating for food packaging applications by using the spray-assisted LbL assembly of CNF and CNW. These two respective nanomaterials, which originate from the two most abundant biopolymers, possess abundant and opposite surface charges, affording effective ionic cross-links within the multilayer to form a hydration-resistant and mechanically stable coating. Owing to their crystallinity and complementary dimensions, this crab-on-a-tree coating minimizes the defects that promote gas permeation, resulting in outstanding oxygen barrier performance that could be used to cover most types of food packaging. We anticipate that these findings will provide insights on the use of abundant cellulose and chitin as well-suited building blocks for LbL coatings and also as a gas barrier coating for food packaging with a variety of functions appealing to the customer, including optical/digital labeling, radio frequency transmission to track food packaging, and antibacterial properties.

METHODS

Materials. An aqueous dispersion of cellulose nanofiber (CNF), which possesses a negatively charged sodium carboxylate group by a surface modification using 2,2,6,6-tetramethyl-1-piperidinyloxy (TEMPO)-mediated oxidation, was purchased from the University of Maine (ME, USA) and used without any further purification. In a typical method, 5 g of cellulose pulp was dispersed in 500 mL of TEMPO solution, which was prepared by dissolving 80 mg of TEMPO and 500 mg of NaBr in 500 mL of deionized water. A 12% aqueous solution of NaClO (37 mL) was slowly added to the mixture. The aqueous CNF dispersion was homogenized with a 750 W ultrasonic processor (Sonics, Vibra-Cell, USA). The dispersion was ultrasonicated for 5 min (pulse on and off for 10 and 5 s, respectively) at an amplitude of 50% in an ice bath. The pH of the reaction medium gradually decreased and was maintained at 10 by the dropwise addition of 0.50 M NaOH solution. This process transformed the primary hydroxyl groups on the CNF surface to carboxylate groups. The pH of the CNF dispersion was adjusted to 7 by adding a few drops of 1.0 M HCl solution.

CNWs were prepared using a slight modification of the method described by Nair and Dufresne.[17] Initially, α-chitin powder from shrimp shell was purchased from Sigma-Aldrich. The α-chitin (5 g) was hydrolyzed in 150 mL of 3 M HCl solution at 120 °C for 3 h and then fully washed with deionized water. Surface deacetylation was accomplished by immersing the hydrolyzed chitin powder in 300 mL of a 30% NaOH solution and heating at 80 °C for 6 h.[18] The product was vigorously washed with distilled water, dialyzed for 3 days until

DOI: 10.1021/acsnano.8b08522
ACS Nano 2019, 13, 3796−3805

the pH reached 7, and freeze-dried. The CNW was redispersed in 50 mM of aqueous acetic acid solution and ultrasonicated for 5 min in an ice bath at the aforementioned setting of the ultrasonic processor. The final pH was adjusted to 3.6 by adding a few drops of 1.0 M HCl solution.

Silicon wafer substrates were cleaned in a piranha solution (H_2SO_4:H_2O_2 7:3 v/v) for 1 h and rinsed with and stored in DI water. *Caution! Piranha solution is dangerous and extremely reactive with organic substances.* Prior to use, the piranha-cleaned silicon wafers were rinsed by sonication in DI water, acetone, and ethanol, respectively, for 10 min each. PET films with a thickness of 50 μm were kindly provided by SKC (Korea). PET film coated with aluminum (300 nm) was purchased from Goodfellow Cambridge Ltd. (Huntingdon, England).

Spray Layer-by-Layer Coating and Hot-Pressing Processes. Spray LbL coating was conducted with an automatic spray coater, NCS-200 (NCS Co. Ltd., Korea). Both the CNW and CNF solutions were diluted to a 0.08 wt % concentration, and the pH was adjusted to 3.6 for CNW and 7.0 for CNF, respectively, with the addition of either 1.0 M HCl or NaOH solution. A PET substrate (13 cm × 13 cm) was fixed on a hot plate with Kapton tape, and the surface temperature was maintained at 80 °C throughout the entire coating process to evaporate the solvent. Two nozzles, through which the respective CNW and CNF solutions passed at a rate of 1.0 mL/min, were employed to spray the solutions on the upper surface of the substrate while moving in a zigzag pattern (50 mm/s) in turn. Each layer comprised five sprayings of each suspension (Figure S11, see Video S1). During the spray LbL assembly, an additional layer was alternatively deposited onto the surface of the receiving layer, completing a single bilayer structure. For example, the sequential assembly of CNW and CNF afforded a bilayer of $(CNW/CNF)_1$. Finally, PET films coated with the bilayers were subjected to hot-pressing at 80 °C at 32 MPa for 10 min.

Characterizations. Based on ASTM 1434-82, the oxygen transmission rate (OTR) was measured using a manometric gas permeation analyzer (Lyssy L100-5000, Systech Illinois Instruments, UK) at 23 °C and 0% RH. The film sample (10 cm × 10 cm) was affixed to the self-adhesive paper holder provided by Systech Instruments. The sample holder, which separated the upper (pure oxygen) and lower (vacuum) chambers, was inserted into the test chamber. This arrangement ensured that 0% RH was created by the pure oxygen and vacuum environments. Prior to the OTR measurement, the films were conditioned to <10% RH in a desiccator for at least 24 h. However, in the hydration resistance test, the humidity conditioning process was not conducted for the $(CNW/CNF)_{40}$-coated PET, as it had been immersed in DI water. The OTR data of triplicate films represent the mean ± standard deviation with statistical significance by the *t*-test. A UV−vis-NIR spectrometer (Cary 5000, Agilent) with a diffuse reflectance accessory (DRA) was used to measure transmittance and haziness. The transmittance and haziness were calculated with eqs 1 and 2 by measuring four types of transmittance: $T1$ (incident light), $T2$ (total light transmitted by sample), $T3$ (light scattered by instrument), and $T4$ (light scattered by instrument and sample). The results are reported for an average value of 9 films of each sample with the standard deviation.

$$\text{transmittance}\,(\%) = \frac{T2}{T1} \times 100 \tag{1}$$

$$\text{haze}\,(\%) = T4 - \frac{T3 \times \frac{T2}{T1}}{T1} \times 100 \tag{2}$$

A Zetasizer Nano ZS device (Malvern, UK) was employed to characterize the surface charge of cellulose and chitin nanomaterials. Suspensions of CNW and CNF nanomaterials were prepared at 0.1 wt % in 50 mM acetate buffer at pH 4 and 7, respectively. The dimensions of the CNWs and CNFs and the surface roughness of the multilayer coatings were measured by AFM (Multimode V, Veeco, USA). The thicknesses of the coated films on silicon wafers were measured by a surface profilometer (Dektak XT, USA). The profilometer determined the thickness by measuring the height difference between the film surface and bare substrate. At least five different positions were measured, and the average thickness value was reported with the standard deviation. The thickness and side morphology of the multilayer-coated PET were examined by scanning electron microscopy (SEM) (SU8220, Hitachi, Japan) at an accelerating voltage of 5 kV. The multilayer-coated PET film was molded in epoxy resin to affix the soft PET film then cut off using a diamond knife.

Antibacterial Property. The bare PET film, CNF- and CNW-coated PET films, and LbL-coated PET films (circular with a diameter of 7 mm) were exposed to *E. coli* and *B. subtilis*. Bacteria-containing aqueous suspensions in log-phase were incubated at 37 °C until the OD_{600} reached 0.6. Then, 50 μL of the respective suspensions was placed on the surfaces of bare, CNW_{40}, CNF_{40}, and $(CNW/CNF)_{20}$-coated PET and incubated for 1 h. The remaining solution on the surface was removed by washing with deionized water, and each film was respectively submerged in fresh Luria−Bertani (LB) nutrient media. Then, the nutrient medium containing each of the films was incubated at 37 °C for 48 h. The regrowth of bacterial cells was evaluated by measuring the OD_{600} at various time points until 48 h. As a negative control, bare PET that was not exposed to the bacteria was used.

QR Code and Radio Frequency Identification Test. An image with KRICT and UNIST symbols was transformed into a QR code using a QR code generator (https://www.qr-code-generator.com). The QR code reader software was operated on a smartphone (Samsung Galaxy S8, Korea). If the software optically recognizes the QR code *via* the camera, then the device displays the image on the screen. A RFID system is composed of a passive tag and a reader. Bare PET, $(CNW/CNF)_{20}$-coated PET, and commercial Al-coated PET films were placed in between the RFID tag and reader. The green and red lights on the reader, respectively, indicate whether the reader succeeded in reading through the PET film and the tag.

Rear Projected Hologram Image. The haziness of the coated films was visualized with a purpose-designed system equipped with a transparent rear projection screen.[37] In a dark room, an image of the KRICT and UNIST logos was projected using a typical beam projector (LG PW1000, Korea). The films were placed in front of the projector at a distance of 30 cm. The hologram images were observed on the opposite side of the projector and recorded by a camera (Samsung Galaxy S8, Korea).

Oxygen Indicator Test. Resazurin is a commonly used oxygen indicator dye that changes to purple in the presence of oxygen.[38] An oxygen-free resazurin solution (1.0 mg/L) was prepared in deionized water and flushed with continuous N_2 flow for 3 h. The colorless resazurin solution was transferred under continuous N_2 flow to a 10 mL vial with a screw cap containing a rubber septum. The pristine and coated PET films were tightly sealed on the septa of the vial cap. A laboratory vacuum pump was employed for 5 min to create negative pressure (5 Torr) in the vial, which was immediately closed by tightening the aluminum cap and sealed with a paraffin film. The color of the solution in each vial was monitored for 4 days.

Bending Test. The resistance toward mechanical stress was evaluated by mounting LbL multilayer-coated PET at each end of a custom-made bending test machine. One of the ends was fixed and the other was moved toward the fixed side at a speed of 60 cm min^{-1}. The machine was paused for 1 s when the bending radius became 11.5 cm, and then the movable side was returned to the starting position, followed by another 1 s pause. This step corresponds to 1 cycle, and the overall bending test comprised 200 cycles.

Effects of Various Harsh Conditions on Crab-on-Tree-Coated PET. The OTR values of $(CNW/CNF)_{20}$-coated PET film were measured after exposure to various harsh conditions: (1) 1 year aging; (2) freezing at −20 °C for 24 h; (3) exposure to ethanol for 1 h; and (4) heating in a microwave oven (800 W) for 5 min.

***In Vitro* Biocompatibility Test.** To evaluate the cytotoxicity of the crab-on-tree coating, the following *in vitro* assay was conducted. The bare and $(CNW/CNF)_{20}$-coated PET films were sterilized with UV for 6 h and then placed in a 24-well plate. A mouse pre-osteoblast

DOI: 10.1021/acsnano.8b08522
ACS Nano 2019, 13, 3796−3805

cell line, MC3T3-E1, was purchased from ATCC (USA) and cultured in minimal essential medium-alpha (MEM-α; Hyclone, Cramlington, UK) with 10% fetal bovine serum (Hyclone, Cramlington, UK) and 1% penicillin/streptomycin (Hyclone, Cramlington, UK) at 37 °C under a humidified atmosphere of 5% CO_2. The subconfluent cells were detached using 0.25% trypsin-EDTA (Hyclone, Cramlington, UK), and the viable cells were counted using a trypan blue assay. The precultivated cells were seeded onto film-containing and empty wells as a control in a 24-well plate at a density of approximately 3×10^4 cells per well and cultured for 3 days in the same nutrient medium. The number of viable cells was determined as a function of culture time (0−3 days) *via* a colorimetric assay (CCK-8, Dojindo, Santa Clara, CA, USA); the number of viable cells is proportional to the light absorbance value (or optical density, OD) at 450 nm. The results given are the mean of triplicate samples and the standard deviation.

ASSOCIATED CONTENT

Supporting Information

The Supporting Information is available free of charge on the ACS Publications website at DOI: 10.1021/acsnano.8b08522.

Characterization data of drying temperature effect, absorption coefficient, AFM, FT-IR, cross-sectional SEM, bending test, extreme condition tests, and antibacterial properties. Table of performance comparison with literatures (PDF)

Video S1: Clip of the spraying process (AVI)

AUTHOR INFORMATION

Corresponding Authors

*E-mail: bskim19@yonsei.ac.kr.

*E-mail: dongyeop@krict.re.kr.

ORCID

Taehyung Kim: 0000-0003-4518-335X

Thang Hong Tran: 0000-0001-7552-1933

Sung Yeon Hwang: 0000-0002-4618-2132

Jeyoung Park: 0000-0002-9369-1597

Dongyeop X. Oh: 0000-0003-3665-405X

Byeong-Su Kim: 0000-0002-6419-3054

Author Contributions

⊥These authors contributed equally.

Notes

The authors declare no competing financial interest.

ACKNOWLEDGMENTS

D.X.O. acknowledges funding from Korea Research Institute of Chemical Technology through Core Program (SI1809, KK1806) and the Technical Cooperation Project of Ulsan Metropolitan City-KRICT (SKO18US02). B.-S.K. acknowledges the financial support by the National Research Foundation of Korea (NRF-2017R1A2B3012148 and NRF-2018R1A5A1025208) and by the Ministry of Trade, Industry, and Energy (MOTIE), Institute for Advancement of Technology (KIAT) through the Encouragement Program for The Industries of Economic Cooperation Region (R&D, R0004883).

REFERENCES

(1) Marsh, K.; Bugusu, B. Food Packaging-Roles, Materials, and Environmental Issues. *J. Food Sci.* **2007**, *72*, R39−R55.

(2) Wang, L.; Kwok, S. K.; Ip, W. H. A Radio Frequency Identification and Sensor-Based System for the Transportation of Food. *J. Food Eng.* **2010**, *101*, 120−129.

(3) Montanari, S.; Roumani, M.; Heux, L.; Vignon, M. R. Topochemistry of Carboxylated Cellulose Nanocrystals Resulting from TEMPO-Mediated Oxidation. *Macromolecules* **2005**, *38*, 1665−1671.

(4) Saito, T.; Kimura, S.; Nishiyama, Y.; Isogai, A. Cellulose Nanofibers Prepared by TEMPO-Mediated Oxidation of Native Cellulose. *Biomacromolecules* **2007**, *8*, 2485−2491.

(5) Ifuku, S. Chitin and Chitosan Nanofibers: Preparation and Chemical Modifications. *Molecules* **2014**, *19*, 18367−18380.

(6) Zeng, J.-B.; He, Y.-S.; Li, S.-L.; Wang, Y.-Z. Chitin Whiskers: An Overview. *Biomacromolecules* **2012**, *13*, 1−11.

(7) Wang, J.; Gardner, D. J.; Stark, N. M.; Bousfield, D. W.; Tajvidi, M.; Cai, Z. Moisture and Oxygen Barrier Properties of Cellulose Nanomaterial-Based Films. *ACS Sustainable Chem. Eng.* **2018**, *6*, 49−70.

(8) Aulin, C.; Gällstedt, M.; Lindström, T. Oxygen and Oil Barrier Properties of Microfibrillated Cellulose Films and Coatings. *Cellulose* **2010**, *17*, 559−574.

(9) Ferrer, A.; Pal, L.; Hubbe, M. Nanocellulose in Packaging: Advances in Barrier Layer Technologies. *Ind. Crops Prod.* **2017**, *95*, 574−582.

(10) Fukuzumi, H.; Saito, T.; Iwata, T.; Kumamoto, Y.; Isogai, A. Transparent and High Gas Barrier Films of Cellulose Nanofibers Prepared by TEMPO-Mediated Oxidation. *Biomacromolecules* **2009**, *10*, 162−165.

(11) Wu, J.; Zhang, K.; Girouard, N.; Meredith, J. C. Facile Route to Produce Chitin Nanofibers as Precursors for Flexible and Transparent Gas Barrier Materials. *Biomacromolecules* **2014**, *15*, 4614−4620.

(12) Richardson, J. J.; Cui, J.; Björnmalm, M.; Braunger, J. A.; Ejima, H.; Caruso, F. Innovation in Layer-by-Layer Assembly. *Chem. Rev.* **2016**, *116*, 14828−14867.

(13) Laufer, G.; Kirkland, C.; Cain, A. A.; Grunlan, J. C. Clay−Chitosan Nanobrick Walls: Completely Renewable Gas Barrier and Flame-Retardant Nanocoatings. *ACS Appl. Mater. Interfaces* **2012**, *4*, 1643−1649.

(14) Yang, Y.-H.; Bolling, L.; Priolo, M. A.; Grunlan, J. C. Super Gas Barrier and Selectivity of Graphene Oxide-Polymer Multilayer Thin Films. *Adv. Mater.* **2013**, *25*, 503−508.

(15) Priolo, M. A.; Gamboa, D.; Holder, K. M.; Grunlan, J. C. Super Gas Barrier of Transparent Polymer−Clay Multilayer Ultrathin Films. *Nano Lett.* **2010**, *10*, 4970−4974.

(16) Priolo, M. A.; Holder, K. M.; Guin, T.; Grunlan, J. C. Recent Advances in Gas Barrier Thin Films *via* Layer-by-Layer Assembly of Polymers and Platelets. *Macromol. Rapid Commun.* **2015**, *36*, 866−879.

(17) Gopalan Nair, K.; Dufresne, A. Crab Shell Chitin Whisker Reinforced Natural Rubber Nanocomposites. 1. Processing and Swelling Behavior. *Biomacromolecules* **2003**, *4*, 657−665.

(18) Fan, Y.; Saito, T.; Isogai, A. Individual Chitin Nano-Whiskers Prepared from Partially Deacetylated α-Chitin by Fibril Surface Cationization. *Carbohydr. Polym.* **2010**, *79*, 1046−1051.

(19) Xiang, F.; Givens, T. M.; Grunlan, J. C. Fast Spray Deposition of Super Gas Barrier Polyelectrolyte Multilayer Thin Films. *Ind. Eng. Chem. Res.* **2015**, *54*, 5254−5260.

(20) Richardson, J. J.; Bjornmalm, M.; Caruso, F. Technology-Driven Layer-by-Layer Assembly of Nanofilms. *Science* **2015**, *348*, aaa2491.

(21) Ajji, A.; Guèvremont, J.; Cole, K. C.; Dumoulin, M. M. Orientation and Structure of Drawn Poly(ethylene Terephthalate). *Polymer* **1996**, *37*, 3707−3714.

(22) Jamieson, E. H. H.; Windle, A. H. Structure and Oxygen-Barrier Properties of Metallized Polymer Film. *J. Mater. Sci.* **1983**, *18*, 64−80.

(23) Henry, B.; Erlat, A.; McGuigan, A.; Grovenor, C. R.; Briggs, G. A.; Tsukahara, Y.; Miyamoto, T.; Noguchi, N.; Niijima, T. Characterization of Transparent Aluminium Oxide and Indium Tin Oxide Layers on Polymer Substrates. *Thin Solid Films* **2001**, *382*, 194−201.

DOI: 10.1021/acsnano.8b08522
ACS Nano 2019, 13, 3796−3805

(24) Lange, J.; Wyser, Y. Recent Innovations in Barrier Technologies for Plastic Packaging - a Review. *Packag. Technol. Sci.* **2003**, *16*, 149−158.
(25) Nakaya, M.; Uedono, A.; Hotta, A. Recent Progress in Gas Barrier Thin Film Coatings on PET Bottles in Food and Beverage Applications. *Coatings* **2015**, *5*, 987−1001.
(26) Buntinx, M.; Willems, G.; Knockaert, G.; Adons, D.; Yperman, J.; Carleer, R.; Peeters, R. Evaluation of the Thickness and Oxygen Transmission Rate before and after Thermoforming Mono- and Multi-Layer Sheets into Trays with Variable Depth. *Polymers* **2014**, *6*, 3019−3043.
(27) Weber, J. W.; Calado, V. E.; van de Sanden, M. C. M. Optical Constants of Graphene Measured by Spectroscopic Ellipsometry. *Appl. Phys. Lett.* **2010**, *97*, 91904.
(28) Johnson, P. B.; Christy, R. W. Optical Constants of the Noble Metals. *Phys. Rev. B* **1972**, *6*, 4370−4379.
(29) Eldesouky, A.; Pulido, A. F.; Mesias, F. J. The Role of Packaging and Presentation Format in Consumers' Preferences for Food: An Application of Projective Techniques. *J. Sens. Stud.* **2015**, *30*, 360−369.
(30) Grande, R.; Trovatti, E.; Carvalho, A. J. F.; Gandini, A. Continuous Microfiber Drawing by Interfacial Charge Complexation between Anionic Cellulose Nanofibers and Cationic Chitosan. *J. Mater. Chem. A* **2017**, *5*, 13098−13103.
(31) Kim, D.; Kwon, H.; Seo, J. EVOH Nanocomposite Films with Enhanced Barrier Properties under High Humidity Conditions. *Polym. Compos.* **2014**, *35*, 644−654.
(32) Pang, Z.; Chen, Q.; Han, W.; Zheng, L. Value-Centric Design of the Internet-of-Things Solution for Food Supply Chain: Value Creation, Sensor Portfolio and Information Fusion. *Inf. Syst. Front.* **2015**, *17*, 289−319.
(33) Shahzad, F.; Alhabeb, M.; Hatter, C. B.; Anasori, B.; Man Hong, S.; Koo, C. M.; Gogotsi, Y. Electromagnetic Interference Shielding with 2D Transition Metal Carbides (MXenes). *Science* **2016**, *353*, 1137−1140.
(34) Benhabiles, M. S.; Salah, R.; Lounici, H.; Drouiche, N.; Goosen, M. F. A.; Mameri, N. Antibacterial Activity of Chitin, Chitosan and Its Oligomers Prepared from Shrimp Shell Waste. *Food Hydrocolloids* **2012**, *29*, 48−56.
(35) Smith, R. J.; Moule, M. G.; Sule, P.; Smith, T.; Cirillo, J. D.; Grunlan, J. C. Polyelectrolyte Multilayer Nanocoating Dramatically Reduces Bacterial Adhesion to Polyester Fabric. *ACS Biomater. Sci. Eng.* **2017**, *3*, 1845−1852.
(36) Ma, H.; Burger, C.; Hsiao, B. S.; Chu, B. Nanofibrous Microfiltration Membrane Based on Cellulose Nanowhiskers. *Biomacromolecules* **2012**, *13*, 180−186.
(37) Brandl, P.; Haller, M.; Hurnaus, M.; Lugmayr, V.; Oberngruber, J.; Oster, C.; Schafleitner, C.; Billinghurst, M. An Adaptable Rear-Projection Screen Using Digital Pens and Hand Gestures. Proceedings from the *17th International Conference on Artificial Reality and Telexistence (ICAT 2007)*, Esbjerg, Jylland, Denmark, November 28−30, 2007; IEEE: Piscataway, NJ, 2007; pp 49−54. http://www.ieee.org (accessed August 29, 2018).
(38) Dietrich, N.; Hebrard, G. Visualisation of Gas-Liquid Mass Transfer around a Rising Bubble in a Quiescent Liquid Using an Oxygen Sensitive Dye. *Heat Mass Transfer* **2018**, *54*, 2163−2171.

DOI: 10.1021/acsnano.8b08522
ACS Nano 2019, 13, 3796−3805